

OSCILLATORY INSTABILITIES AND FIELD DOMAIN FORMATION IN IMPERFECT SUPERLATTICES

E. Schöll, G. Schwarz, M. Patra, F. Pregel, and A. Wacker

Institut für Theoretische Physik, Technische Universität Berlin,
Hardenbergstraße 36, 10623 Berlin, Germany

We theoretically investigate vertical high-field transport in semiconductor superlattices, which exhibit self-generated current oscillations and the formation of stable stationary electric field domains depending on the available carrier density. We demonstrate that this behavior is strongly affected by growth-related imperfections like fluctuations of the doping density, the well and the barrier widths. We propose to use this as a novel noninvasive method to detect growth-related disorder in superlattices.

INTRODUCTION

We consider a semiconductor superlattice where electric field domains form in the growth direction under high-field conditions if the superlattice is sufficiently doped or optically excited¹⁻⁴. Previous studies have shown that the current-voltage characteristic consists of a sequence of branches (their number being roughly equal to the number of quantum wells), which arise from different locations of the domain boundary. These branches overlap in a certain range of the voltage, leading to multistability and different curves for sweep-up and sweep-down of the voltage⁵. Recently, time-dependent features like transient⁶ and persistent⁷ oscillations have also been observed and reproduced by different models of structurally “perfect” superlattices^{8,9}.

The model used here is an extension of the approach presented in Refs.^{10,8} for a “perfect” superlattice consisting of N GaAs quantum wells separated by $N - 1$ AlAs barriers. Here we study imperfections associated with frozen-in fluctuations of the doping and the well and barrier widths in the growth direction only. We denote by b_i the width of the i^{th} barrier, which is located between the i^{th} and $(i - 1)^{\text{st}}$ well of widths l_i and l_{i-1} , respectively. The wells are n-doped with a doping concentration (per unit volume) $N_D^{(i)}$ in the i^{th} well. We define a “local” lattice constant $d_i := b_i + (l_i + l_{i-1})/2$ to describe the vertical transport across the i^{th} barrier. For simplicity we consider only the two lowest subbands, $k = 1, 2$. The rate of change of the carrier densities $n_k^{(i)}$ (per unit area) in the k^{th} subband of the i^{th} well is given by

$$\dot{n}_1^{(i)} = n_2^{(i)}/\tau_{21} + R_1^{(i)} n_1^{(i-1)} - R_1^{(i+1)} n_1^{(i)} - n_1^{(i)} (X_r^{(i+1)} + X_l^{(i)}) + n_2^{(i+1)} Y_l^{(i+1)} + n_2^{(i-1)} Y_r^{(i)} \quad (1)$$

$$\dot{n}_2^{(i)} = -n_2^{(i)}/\tau_{21} + R_2^{(i)} n_2^{(i-1)} - R_2^{(i+1)} n_2^{(i)} - n_2^{(i)} (Y_l^{(i)} + Y_r^{(i+1)}) + n_1^{(i-1)} X_r^{(i)} + n_1^{(i+1)} X_l^{(i+1)} \quad (2)$$

where $\tau_{21} = 1$ ps is the intersubband relaxation time, $R_k^{(i)}$ is the rate of electrons crossing the i^{th} barrier between equivalent subbands k of two neighbouring wells modelled by miniband conduction¹⁰.

The tunnelling coefficients $X_r^{(i)}$, $X_l^{(i)}$, $Y_r^{(i)}$, and $Y_l^{(i)}$ for transitions between different subbands of neighbouring wells depend on the field $F^{(i)}$; the subscripts r and l denote resonant tunnelling to the right and left, respectively. X stands for transitions from the first to the second subband, and Y for the reverse process. They are calculated from perturbation theory¹⁰, but using local energy levels and barrier widths. $X_r^{(i)}$ and $Y_l^{(i)}$ exhibit a distinct maximum for large electric fields where the first and the second subband of adjacent wells are in resonance. The electric field $F^{(i)}$ can be calculated from Poisson's law $\epsilon(F^{(i+1)} - F^{(i)}) = e(n_1^{(i)} + n_2^{(i)} - l_i N_D^{(i)})$, where ϵ is the permittivity of GaAs. The fields have to satisfy $\sum_{i=1}^{N+1} d_i F^{(i)} = U$, where U is the voltage applied to the sample. The sample contacts are treated as two additional "virtual" wells denoted by 0 and $N + 1$, for which the boundary conditions $n_i^{(0)} = n_i^{(1)}$ and $n_i^{(N+1)} = n_i^{(N)}$ are assumed.

SIMULATIONS

For uniform electric fields the current-voltage characteristic following from (1), (2) exhibits a two-peak-structure with a sharp maximum due to resonant tunneling. However, this characteristic with a regime of negative differential conductivity (NDC) is stable only at low doping. At higher doping, spatio-temporal instabilities lead to self-oscillations of the current associated with the build-up of space-charges^{8,11}. At the highest doping densities, the number of available carriers is sufficient to provide the space charge necessary to form a stable boundary between a low-field and a high-field domain. Stationary domains are then found. This behavior is summarized in Fig. 1 for a "perfect" superlattice. The inset depicts a bifurcation scenario for fixed N_D where limit cycle oscillations are generated from the inhomogeneous branch by a supercritical Hopf bifurcation H_{super} . The amplitude of the current oscillations is indicated by the hatched area. There is a small regime of bistability between the inhomogeneous steady state and the oscillations beyond the subcritical Hopf bifurcation H_{sub} . T denotes transcritical bifurcations of various steady states. Fig. 2 (a) shows the periodic oscillations for intermediate doping. The homogeneous field distribution breaks up into a low- and a high-field domain. The latter shrinks while at the same time its field grows rapidly forming a steep but unstable domain wall. This leads to a sharp rise of the current. When the current has reached a certain value the high-field domain collapses, resulting in the original quasi-homogeneous field distribution. This process is repeated periodically. When a small amount of doping fluctuations is introduced (Fig. 2 (b)) the spatially homogeneous phase of the field distribution decreases resulting in more sinusoidal oscillations of the current

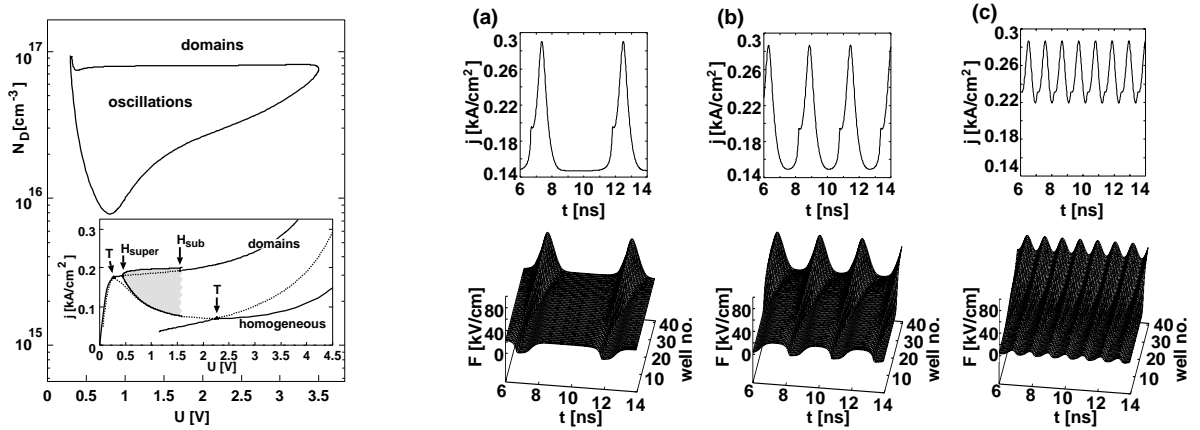


Figure 1: (left) Phase diagram of spatio-temporal instabilities as a function of doping density N_D and bias voltage U for a perfect superlattice of $N = 40$ periods of GaAs/AlAs layers with $l = 90 \text{ \AA}$, $b = 15 \text{ \AA}$. The inset shows a bifurcation scenario for fixed $N_D = 2 \cdot 10^{16} \text{ cm}^{-3}$ (full lines: stable steady states, dotted lines: unstable steady states, hatched area: limit cycle oscillations)

Figure 2: (right) Self-oscillations with $N_D = 3 \cdot 10^{16} \text{ cm}^{-3}$ at $U = 1 \text{ V}$ (a) for a perfect superlattice, (b) for doping fluctuations of $\alpha = 0.1\%$, (c) for $\alpha = 3\%$, where $N_D^{(i)} = N_D(1 + \alpha e_i)$ with a random set of N values e_i from the interval $[-1, 1]$. The current density j versus time t and the evolution of the field distribution $F(x, t)$ are shown.

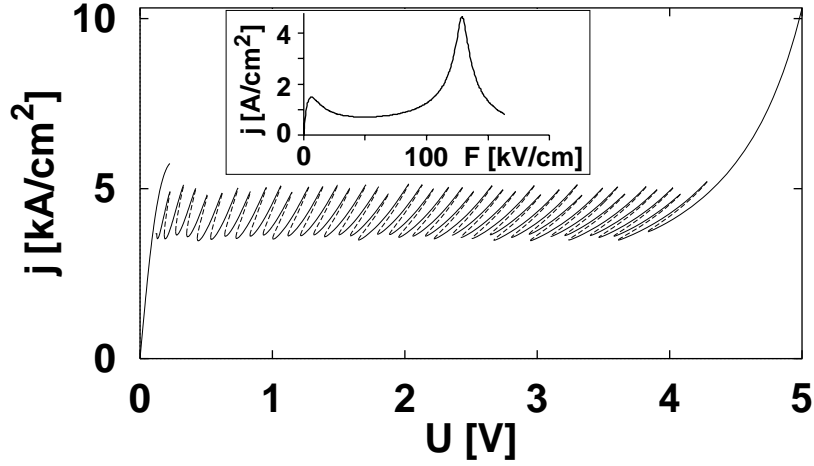


Figure 3: Current density j vs. voltage U for $N_D = 6.7 \cdot 10^{17} \text{ cm}^{-3}$ and doping fluctuations of $\alpha = 3\%$. Both stable (full) and unstable (dashed) domain states are shown. The inset depicts the current-voltage characteristics for uniform fields.

and a higher frequency. For larger fluctuations (Fig. 2 (c)) the homogeneous part vanishes completely, since the presence of irregularities supports the formation of charge accumulations. Furthermore, at doping concentrations N_D for which the perfect superlattice would exhibit damped oscillations which asymptotically tend to a stable domain field distribution, we find persistent self-generated oscillations above a certain threshold of disorder. The actual shape of the boundary between both regimes, however, depends sensitively on the individual sequence of the irregularities. It is even possible that a sample with a particular spatial sequence of fluctuations shows stable domains, while the inverted sequence (corresponding to reversed bias) leads to self-oscillations.

In Fig. 3 the current-voltage characteristic is shown at a higher mean doping density where stable stationary high-field domains form at the anode in the NDC regime (cf. inset). In contrast to earlier work we have displayed here the full connected current-voltage characteristic. Along the characteristic stable and unstable parts alternate. They correspond to a continuous shift of the domain boundary across the superlattice from the anode ($i = N$) to the cathode ($i = 1$) with on average increasing bias. On the i^{th} stable part (with rising voltage) the domain boundary is pinned at the $(N - i)^{\text{th}}$ well, while along the unstable parts (with falling voltage) the boundary is shifted to the next well. For neighbouring stable branches the domain boundary is thus displaced by one superlattice period. The irregularly varying length of the different branches is due to the doping fluctuations which determine the maximum and minimum current. Upon voltage sweep-up or sweep-down only parts of the stable branches can be reached (Fig. 4 (a)). With increasing degree of disorder, the irregularities are enhanced, and some stable branches are missed out altogether, as a result of their reduced length. The characteristics are in good agreement with the experiments⁵ and allow even an estimate of the range of doping fluctuations between 3–10%.

In Fig. 4 (b) monolayer fluctuations of well and barrier widths are studied. In (α) the 18^{th} well is chosen to be larger by one monolayer, while in (β) two wells are larger (the 11^{th} and the 32^{nd}), and two wells are smaller (the 12^{th} and the 18^{th}) by one monolayer. In (γ) there are four larger and four smaller wells. Finally, in (δ) the 31^{st} barrier is wider by one monolayer. For increasing disorder (α)–(γ), we find the sequence of branches to exhibit a more and more irregular behavior. When only a small number of irregularities is present, it is even possible to determine their location within the superlattice structure. When at higher voltages a high-field domain forms near the anode (well no. 40) its influence becomes visible in the current-voltage characteristic only if the domain boundary crosses the barriers close to the perturbation. In this case the transition of the associated charge accumulation layer from one well into the next one occurs at a smaller or a larger applied voltage compared to the case of the perfect superlattice. This results in an extension or reduction, respectively, of the length of that current branch. It is thus possible to determine the location of a single irregularity of the well width from the current-voltage characteristic by enumerating the branches. (Fig. 4 (b)). If two perturbations are well

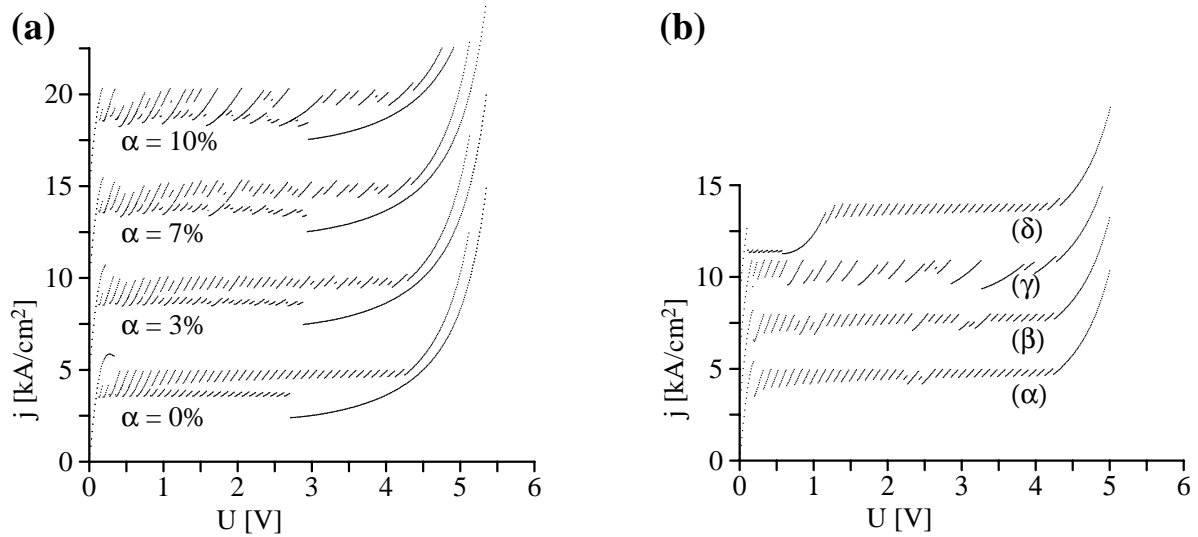


Figure 4: (a) Current-voltage characteristics for voltage sweep-up and sweep-down with different doping fluctuations. (b) Voltage sweep-up with different imperfections of wells and barriers. ($N_D = 6.7 \cdot 10^{17} \text{ cm}^{-3}$; the vertical scale is shifted for each curve)

separated within the superlattice structure so that the regions where they affect the field distribution do not overlap, their influences can still be distinguished. If the number of irregularities increases, their interaction leads to a more complex behavior in the corresponding part of the current-voltage characteristic (γ). The widths of the barriers can also severely affect the current-voltage characteristic, which can be seen in (δ) where the 31st barrier is wider by one monolayer. The voltage at which the domain boundary crosses the perturbation (i. e. the location of the perturbation within the superlattice) can be easily detected from the characteristic.

In conclusion, we propose to use macroscopic nonlinear transport properties far from equilibrium as a novel, noninvasive method of probing growth-related disorder and imperfections in superlattices. By simple global macroscopic electric measurements, in combination with model calculations, microscopic structural features can thus be investigated.

We thank L. Bonilla, H. T. Grahn, and J. Kastrup for enlightening discussions. This work was supported by DFG in the framework of Sfb 296.

REFERENCES

1. L. Esaki and L. L. Chang, Phys. Rev. Lett. **33**, 495 (1974).
2. K. K. Choi, B. F. Levine, R. J. Malik, J. Walker, and C. G. Bethea, Phys. Rev. B **35**, 4172 (1987).
3. H. T. Grahn, R. J. Haug, W. Müller, and K. Ploog, Phys. Rev. Lett. **67**, 1618 (1991).
4. Y. Zhang, X. Yang, W. Liu, P. Zhang, and D. Jiang, Appl. Phys. Lett. **65**, 1148 (1994).
5. J. Kastrup, H. T. Grahn, K. Ploog, F. Prengel, A. Wacker, and E. Schöll, Appl. Phys. Lett. **65**, 1808 (1994).
6. R. Merlin, S. H. Kwok, T. B. Norris, H. T. Grahn, K. Ploog, L. L. Bonilla, J. Galán, J. A. Cuesta, F. C. Martínez, and J. M. Molera, in *Proc. 22nd Int. Conf. Phys. Semicond.*, edited by D. J. Lockwood (World Scientific, Singapore, 1995), p. 1039.
7. H. T. Grahn, J. Kastrup, K. Ploog, L. L. Bonilla, J. Galán, M. Kindelan, and M. Moscoso, Jpn. J. Appl. Phys. (1995), in press.
8. A. Wacker, F. Prengel, and E. Schöll, in *Proc. 22nd Int. Conf. Phys. Semicond.*, edited by D. J. Lockwood (World Scientific, Singapore, 1995), p. 1075.
9. L. L. Bonilla, J. Galán, J. A. Cuesta, F. C. Martínez, and J. M. Molera, Phys. Rev. B **50**, 8644 (1994).
10. F. Prengel, A. Wacker, and E. Schöll, Phys. Rev. B **50**, 1705 (1994).
11. L. L. Bonilla, in *Nonlinear Dynamics and Pattern Formation in Semiconductors*, edited by F. J. Niedernostheide (Springer, Berlin, 1995), Chap. 1.